This is the Author's Pre-print version of the following article: *C.F. Sánchez-Valdés, R.R. Gimaev, M. López-Cruz, J.L. Sánchez Llamazares, V.I. Zverev, A.M. Tishin, A.M.G. Carvalho, D.J.M. Aguiar, Y. Mudryk, V.K. Pecharsky, The effect of cooling rate on magnetothermal properties of Fe49Rh51, Journal of Magnetism and Magnetic Materials, Volume 498, 2020, 166130,* which has been published in final form at: https://doi.org/10.1016/j.jmmm.2019.166130

© 2020 This manuscript version is made available under the Creative Commons Attribution-NonCommercial-NoDerivatives 4.0 International (CC BY-NC-ND 4.0) license http://creativeco mmons.org/licenses/by-nc-nd/4.0/

The effect of cooling rate on magnetothermal properties of $Fe_{49}Rh_{51}$

C.F. Sánchez-Valdés,[a] R.R. Gimaev,[b,c] M. López-Cruz,[d] J.L. Sánchez Llamazares,[d,*] V.I. Zverev,[e,**] A.M. Tishin,[c,e] A.M.G. Carvalho,[f] D.J.M. Aguiar,[g] Y. Mudryk, [h] and V.K. Pecharsky [h]

[a]*División Multidisciplinaria, Ciudad Universitaria, Universidad Autónoma de Ciudad Juárez (UACJ), calle José de Jesús Macías Delgado # 18100, Ciudad Juárez 32579, Chihuahua, México*
[b]*National Research Center "Kurchatov Institute" Moscow, 123182, Russia*
[c]*Advanced Magnetic Technologies and Consulting LLC, 142190, Promyshlennaya 4, Troitsk, Russia.*
[d]*Instituto Potosino de Investigación Científica y Tecnológica A.C., Camino a la Presa San José 2055, Col. Lomas 4ª, San Luis Potosí, S.L.P. 78216, México.*
[e]*Faculty of Physics, M.V. Lomonosov Moscow State University, 119991, Leninskie gory 1-2, Moscow, Russia.*
[f]*Departamento de Engenharia Mecânica, Universidade Estadual de Maringá, 87020-900, Maringá, PR, Brazil.*
[g]*Universidade Tecnológica Federal do Paraná, UTFPR, CEP 84017-220, Ponta Grossa, PR, Brazil.*
[h]*Ames Laboratory of the US DOE and Department of Materials Science and Engineering, Iowa State University, Ames, IA 50011-3020, U.S.A.*

* Corresponding author. Instituto Potosino de Investigación Científica y Tecnológica A.C., Camino a la Presa San José 2055 Col. Lomas 4ª sección, San Luis Potosí 78216, San Luis Potosi, México. E-mail address: jose.sanchez@ipicyt.edu.mx (J.L. Sánchez Llamazares; **jose.sanchez@ipicyt.edu.mx**).
** Corresponding author. Faculty of Physics, M.V. Lomonosov Moscow State University, 119991, Leninskie gory 1-2, Moscow, Russia. E-mail address: vi.zverev@physics.msu.ru (Vladimir Zverev; **vi.zverev@physics.msu.ru**).

ABSTRACT. We have investigated the effects of quenching rate on the thermal dependence of the magnetic entropy change $\Delta S_M(T)$ and the magnetic field induced hysteresis loss through the antiferromagnetic (AFM) ↔ ferromagnetic (FM) transformation in bulk $Fe_{49}Rh_{51}$. Two nearly identical square-prism-shaped samples were subjected to two different temperature cooling regimes; one was rapidly quenched (FQ) in iced-water and another slow cooled (SC) to room temperature at a cooling rate of 2 K/min. The temperature of the AFM↔FM transition is similar for both samples, but the FQ sample shows much sharper temperature- and magnetic field-induced magnetization change; in addition, the total magnetization change is 14 % larger. In FQ material, the magnetocaloric effect, i.e., $\Delta S_M(T)$ quickly approaches saturation above 1 T and shows a large peak value at 2 T (13.9 versus 8.9 $Jkg^{-1}K^{-1}$ in SC material), but a larger average hysteresis loss $\langle HL \rangle_{FWHM}$ in the temperature range coinciding with of the full-width at half-maximum of the $\Delta S_M(T)$ curve.

Keywords: Magnetocaloric; magnetic refrigeration, iron-rhodium alloys.
PACS No's: 75.30.Kz, 75.47.Np, 75.90.+w

1. INTRODUCTION.

Nearly equiatomic $Fe_{100-x}Rh_x$ alloys (at. %), i.e., when $48 \leq x \leq 52$ (henceforth FeRh as a group) with the ordered CsCl-type crystal structure (also known as B2 or α' phase) show remarkable magnetocaloric effects (MCEs) near room temperature (RT), which are associated with magnetoelastic first-order antiferromagnetic ↔ ferromagnetic (AFM↔FM) phase transitions [1–5]. Recent theoretical calculations suggest that the cubic B2-type lattice of FeRh exhibits premartensitic instability around RT, and becomes unstable at ambient pressure, transforming martensitically at low temperature into an orthorhombically distorted variant of the B2 structure [6]. Energetically, the orthorhombic structure is only a few meV/atom below that of the ideal cubic B2-type structure. For comparison, this energy difference is more than one order of magnitude lower than the latent heat of the well-documented AFM ↔ FM transition [6]. Earlier experimental results regarding the total entropy, the isothermal entropy change and the adiabatic temperature change, and the structural transition temperature, among other properties of Fe-Rh, agree with the proposed structural model [6].

Structural instabilities, therefore, appear to be intrinsic to Fe-Rh, and they may have a significant impact on their magnetic and magnetocaloric properties. One of the main tasks of this work is to experimentally investigate the influence of crystallographic instabilities on the AFM ↔ FM phase transition and a possible effect of sample history and crystal structure on the magnetic entropy change (ΔS_M) of bulk $Fe_{49}Rh_{51}$. Establishing a clear correspondence between the preparation conditions and the resulting crystal structures is not only interesting fundamentally, but it is critical for the synthesis of Fe-Rh materials with the maximum possible magnetocaloric effects.

The large MCE in the title material originates from a first-order AFM↔FM transition accompanied by exchange inversion associated with a temperature-induced unit cell volume change of approximately 1.0 % while retaining the cubic B2-type symmetry and structure with only minor changes of interatomic distances. The nature of this transition is, therefore, magnetoelastic [7–9]. Originally, the structural, magnetic and magnetocaloric behaviors of both bulk alloys and thin films of Fe-Rh have been broadly investigated in the 1990´s, but over the last few years there has been an uptick of interest in these materials with the main goal to better understand the physical origin(s) of their remarkable magnetocaloric response [5,10–14], which is both of scientific and technological importance. Large magnetic field-induced peak values of both the magnetic entropy change, $|\Delta S_M^{peak}|$, [1,3–5,10] and the adiabatic temperature change, $|\Delta T_{ad}^{peak}|$, of 13 – 20 $Jkg^{-1}K^{-1}$ (here, the electronic contribution can be as high as 8 $Jkg^{-1}K^{-1}$ [15,16]) and 7 - 12.9 K, respectively, for the reference magnetic field change, $\mu_o\Delta H$, of 2 T have been reported. The largest value of ΔT_{ad}^{peak} = -20 K at the magnetic field change of 8 T was also reported in [17]. But the most

significant feature in this sense is the fact that Fe-Rh holds the record in the experimentally measured ΔT_{ad}^{peak} when compared with the values obtained for any other first-order magnetocaloric material [1,18].

Reviewing the literature dedicated to Fe-Rh alloys in bulk form one quickly realizes that there are no systematic studies on the correlation between synthesis parameters and the characteristic features of the AFM↔FM phase transition; this refers to the temperature of the transition, its sharpness and the magnetization jump ΔM, and the effect of the magnetic field on the transition itself [4]. What is even more important, reported results are often difficult to reproduce even following the synthesis conditions described in the published literature. This happened, in fact, during the course of our study. In order to shed light on the origin of the known irreproducibilities, a recent study has drawn attention to the significant effect of local stresses induced through the grain boundary on the B2 phase when it coexists with the fcc γ phase [19]. The latter is a high-temperature solid-solution phase that exists over the entire composition range in the Fe-Rh binary system [20], whose lattice parameter changes depending on composition and thermal treatment [19].

In this work, we focus on the reference composition $Fe_{49}Rh_{51}$, and show that the cooling rate from the thermal annealing temperature (1273 K) strongly affects the sharpness of the first-order AFM↔FM transition with the consequent effect on the resulting $\Delta S_M(T)$ and magnetic hysteresis loss.

2. EXPERIMENTAL.

An alloy with the nominal composition $Fe_{49}Rh_{51}$ was prepared from Rh powder (99.96 wt.% pure; Ames Laboratory) and Fe chips (99.98 wt.% pure; Aldrich). First, Rh powder was cold-pressed into a small pellet. Next, the Rh pellet and Fe chips (weighed to achieve $Fe_{49}Rh_{51}$ stoichiometry) were arc-melted together under high-purity Ar. The sample was re-melted 4 times to ensure a reasonably good starting homogeneity. The overall chemical composition of the as-arc-melted alloy was checked by EDS and it was as-nominal – $Fe_{49}Rh_{51}$ – within the experimental errors of the technique. From the arc melted bulk sample, two square prisms were cut using a Model 650 low speed diamond wheel saw; their approximate dimensions were 0.5 × 0.5 × 3.5 mm^3. Taking into account that the cutting may mechanically damage the surface by transforming the B2-type structure of FeRh into an fcc structure [21], both $Fe_{49}Rh_{51}$ samples were annealed at 1273 K for 48 hours in separate quartz tubes sealed under vacuum. After the heat treatment, one of the samples was fast quenched (henceforth FQ sample) into an ice-water mixture, while the other was slowly cooled (henceforth SC sample) to RT at 2 K/min.

X-ray diffraction (XRD) patterns were collected at room temperature with a Rigaku Smartlab high-resolution diffractometer using Cu-Kα radiation (λ = 1.5405 Å; $20^o \leq 2\theta \leq 90^o$; step increment 0.01^o). The

XRD data were collected by reflecting the X-ray beam from one of the flat surfaces of the annealed square prism-shaped samples. The temperature dependence of the lattice parameter were obtained using the XRD1 beamline at the Brazilian synchrotron light source (LNLS), a detailed description of which is presented in [22].

DSC measurements were carried out on heating and subsequent cooling in the temperature range 200-413 K using the DSC model Q200 from TA instruments; the temperature sweep rates were 10 K/min for both heating and cooling.

Magnetization measurements were performed in a 9 T Quantum Design Dynacool® physical property measurement system (PPMS®) using the vibrating sample magnetometer (VSM) option. For the measurements carried out between 2 and 400 K the square prism-shaped samples were glued directly on a quartz paddle VSM sample holder using GE-7031 varnish, whereas for measurements above 400 K the VSM oven was used and the samples were glued with Duco cement onto a heater stick. The external magnetic field was applied along the major length of the square prism-shaped samples to minimize the effect of the internal demagnetizing field. The magnetization as a function of temperature, $M(T)$, was measured under low ($\mu_o H$ = 5 mT) and high ($\mu_o H$ = 2 T) static magnetic fields from 5 to 400 K and from 400 to 800 K with the heating and cooling rates of 1.0 K/min and 1.5 K/min, respectively. A set of isothermal magnetization $M(\mu_o H)$ curves, was also measured across the AFM ↔ FM transition, from which the magnetic-field induced entropy change as a function of temperature, $\Delta S_M(T)$, was determined by numerically integrating Maxwell relation. The following thermal cycle was followed to measure $M(\mu_o H)$ at each fixed temperature [23]: (i) heating to 400 K in a zero magnetic field followed by cooling to 200 K; (ii) heating again to reach the measurement temperature, T_{meas}. The heating and cooling rates during every cycle were 20 K/min except when approaching T_{meas} during the second heating, where the heating rate was automatically reduced to ensure T_{meas} is not exceeded, i.e., the set points were approached in the no overshoot mode. To ensure stability of T_{meas} above 270 K and, therefore, to achieve true isothermal conditions before each field-dependent measurement, the temperature was stabilized during 15 minutes at every selected T_{meas}. Due to the expected impact of thermal history on measurement results in the vicinity of the AFM↔FM phase transition, all experiments were performed slowly to ensure quasi stable conditions during cooling and heating, magnetization and demagnetization in order to reach the most stable (minimum magnetic energy) magnetic phase.

3. RESULTS AND DISCUSSION

Figures 1(a) and (b) shows the XRD patterns of the two $Fe_{49}Rh_{51}$ samples. The thin surface layer (the data were collected from surfaces of the heat-treated pyramidal samples) of the FQ sample is clearly single-phase with only the Bragg peaks of the B2 (CsCl)-type crystal structure present (see Fig. 1a). We note that both sets of data presented in Figs. 1(a) and (b) are probing no more than ~10 μm depth below the surface considering that the linear absorption coefficient of FeRh for Cu-Kα radiation is ~200 cm^{-1} and assuming that the beam is fully absorbed when its intensity is reduced by a factor of 100. Using extrapolation, the unit cell dimension, a, of the B2 $Fe_{49}Rh_{51}$ phase is 2.991 ± 0.004 Å, which is within two standard deviations from the earlier reported [24] value of 2.981 Å. Bragg peaks of the SC sample (Fig. 1b) are asymmetric, indicating local chemical inhomogeneity. The main phase near the surface of the SC sample is face-centered cubic (fcc), which is the high-temperature phase known to exist in the Fe-Rh binary system [25]. The minority phase is B2 (CsCl)-type, same as in the FQ sample, with a = 2.993 Å which is within experimental error identical to the same in the FQ phase. The majority fcc phase has a = 3.856 Å, substantially higher than one may expect from the unit cell dimensions of both fcc Fe (3.648 Å) and Rh (3.803 Å) and from the earlier reported [26] value of the fcc $Fe_{50}Rh_{50}$ (3.739 Å). At present, we do not have a reasonable explanation for this discrepancy.

As a result of the XRD study in the temperature range of 270 - 380 K (i.e., in the region of the FM↔AFM phase transition in the B2 phase), the temperature dependence of the lattice parameter, both on heating and cooling, for FQ and SC samples was obtained, and is shown in Fig. 1(c). The phase transition is accompanied by a change in the lattice parameter of 0.27% (corresponding to a volume change of 0.81%) for FQ and of 0.36% (corresponding to a volume change of 1.1%) for the SC sample. Both volume changes are commensurate with earlier neutron diffraction studies [7–9,27], which reported around a 1% change in the lattice volume during the transition. The unit cell hysteresis width in Fig. 1(c) is about 20 K, which is larger than the 9-11 K determined from the low field $M(T)$ and 11-12 K from the DSC data shown in Fig. 2(a) and (b). The shift in the transition temperatures relative to the high field $M(T)$ data shown later in Figure 4 is due to the effect of the magnetic field on the magnetoelastic transition of the B2 phase. Noticeable differences are also observed in the behavior of lattice parameters, which begin to change rapidly at approximately 20 K higher temperatures when compared with $M(T)$ under a weak field and DSC data (Figs. 1c and Figs. 2(a) and (b), respectively).

The resulting discrepancies in temperatures indicate that transformations in the magnetic and crystallographic sublattices may not be fully coupled. It also appears that the magnetoelastic transition in the B2 phase of Fe-Rh involves earlier unidentified intermediate state, which is manifested as a nearly constant lattice parameters near the beginning (between 320 and 330 K during heating) and near the end

(between 315 and 322 K during cooling) of the transition.

Figs. 3(a) and (b) show the temperature dependencies of the magnetization for both FQ and SC samples recorded at 5 mT from 2 to 800 K, respectively. Thermal hysteresis associated with the AFM↔FM phase transitions in both samples are 9-11 K, which as broader than ~7.5 K reported recently in Ref. [5]. While it is possible that this difference may be due to the annealing times (48 hours in this work and one week in [5]), it is also feasible that sample shapes played a role (a $5\times3\times1$ mm^3 plate-like sample was used in [5]). The top insets in both figures show details just below the AFM↔FM phase transitions, which are similar for both samples. Gradual rise of $M(T)$ as temperature decreases and minor divergence of the heating and cooling $M(T)$ data are likely related to a gradual relaxation of strain associated with approximately 1% volume change of the B2 phase. The bottom insets are derivatives of magnetizations with respect to temperature measured in the vicinity of paramagnetic (PM)↔FM transition; the corresponding Curie temperatures, T_C, are indicated in the insets. Minor thermal hystereses are experimental artifacts most likely related to both the continuous temperature sweeps and numerical differentiation. The difference in T_Cs of FQ and SC samples is significant, nearly 40 K, and is believed to be related to the observed dominance of the γ-type $Fe_{49}Rh_{51}$ phase in the surface layer of the SC sample and, possibly, to minor fluctuations in the local composition of the arc-melted button, which are quite difficult to detect experimentally.

The comparison of $M(T)$ curves measured under a 2 T magnetic field shown in Fig. 4 points to substantial differences in the progression of the AFM↔FM phase transitions. For the FQ sample the transition is, as expected, much sharper than that in SC sample, which is also highlighted by narrow and broad, respectively, peaks of $dM/dT(T)$ plotted in the inset. In addition, the magnetization change, ΔM = ~133 Am^{2}kg^{-1}, is 14 % larger than the one determined for the SC sample and is close to 134 Am^{2}kg^{-1} at 2 T reported in [5]. We note that even a larger value of around 140 Am^{2}kg^{-1} in magnetic field of 1 T was reported for equiatomic $Fe_{50}Rh_{50}$ whose AFM-FM transition occurs at ~390 K [4]. Ab-initio estimate of the saturation magnetization is 147 Am^{2}kg^{-1} for the ferromagnetic B2-type phase at T = 0 K (3.11 μ_B for Fe and 1.07 μ_B for Rh) [24]. In this model, the AFM↔FM transition occurs at temperature where the ferromagnetic order is about 90% of full collinearity, so the expected magnetization jump of 132 Am^{2}kg^{-1} is in an excellent agreement with respect to the one observed in the FQ sample.

Figure 5(a) compares the typical isothermal magnetization curves measured up to a maximum magnetic field of 2 T through the magnetic field-induced AFM→FM phase transition for both FQ and SC samples. Similar to $M(T)$ curves, $M(\mu_oH)$ are vastly different: metamagnetic-like jumps are both much sharper and much higher in FQ than in SC material. Figure 5(b) shows temperature dependences of the critical fields, μ_oH_{cr}, for the field-induced AFM→FM transition defined as maximum slopes of the measured

$M(\mu_o H)$ data. The critical fields are linear functions of temperature below 2 T with slopes of about -0.12 T/K. This behavior of the critical fields is similar to that determined from magnetostriction measurements of Ref. [28] and it agrees with the $\mu_o H_{cr}(T)$ dependence reported in [29].

Figure 5(b) illustrates that the critical fields of FQ and SC samples are also different. The difference is approximately 2 K at low fields, increasing slightly at 2 T, which is quite consistent with the difference in the transition temperatures of FQ and SC samples seen in the inset of Fig. 4. The difference in the magnitude of the critical field, as mentioned above in the discussion of Fig. 4, is associated with a significant difference in the shape of the hysteresis loop during the transition caused by a delay in the formation of nuclei of the ferromagnetic phase. It should be noted that in zero magnetic field, the transition was observed as high as 423 K in slowly cooled materials [28]. At the same time, we find that in nearly zero magnetic field, the FM state develops at 326 K for FQ and at 329 K for SC samples. Hence, the method of preparation, heat treatment and phase purity, and even minor differences in the alloy composition have a strong effect on the phase transition temperature.

The calculated temperature dependencies of the magnetic entropy change, ΔS_M, and the dependence of the maximum magnetic entropy change ΔS_M^{peak} on the magnetic field change are illustrated in Figs. 6(a) and (b), respectively. Apart from the larger ΔS_M^{peak} value obtained for FQ sample at 2 T owing to the sharper magnetization increase (56 % and 37 % higher than those obtained, respectively, for our SC sample and the sample with the same stoichiometry studied in [1]), above 1 T the maximum entropy change becomes nearly constant giving rise to a progressive table-like shape. The latter is related to the magnetic field change dependence of the temperatures T_{cold} and T_{hot} that define the full-width at half-maximum of the $\Delta S_M(T)$ curve (δT_{FWHM}); Fig. 6(c) shows how these parameters change with $\mu_o \Delta H$ for both alloys. Whereas T_{hot} remains practically constant, T_{cold} decreases rapidly as $\mu_o \Delta H$ increases, explaining the widening of the $\Delta S_M(T)$ curves towards lower temperatures. Figure 6(c) also shows the nearly linear increase of δT_{FWHM} with $\mu_o \Delta H$ for both samples above 0.5 T.

This behavior is due to the nature of FOMT in the studied samples, which is much sharper in the FQ material. Importantly, in a rather weak magnetic field of ~0.5 T, $|\Delta S_M^{peak}|$ reaches 80% of the values observed in much higher magnetic field of 2 T (as the inset of Fig. 6(b) shows). Considering that the large magnetic entropy (and, correspondingly the large adiabatic temperature change) occurs over a few K temperature window in such a small field, appropriately designed Fe-Rh materials can be very effective in fixed temperature applications. One example would be medical use considering a nearly constant body temperature of ~310 K, where quick and substantial cooling (and/or heating) of the surrounding tissue can be triggered by 0.5 – 1 T magnetic fields. Of course, Fe-Rh chemistry must be tuned to exhibit the sharpest

possible magnetoelastic transition at 310 K, and the material must be delivered or implanted where the cooling/heating is required.

We note, however, that the increasing contribution of the paraprocess in magnetic fields much higher than 2 T can change the trends illustrated in Figs. 6(a) and 6(b). Earlier [30] it was shown that the maximum MCE values arising due to the paraprocess, in rare-earth metals in extremely high fields can reach ΔT = 250K with $\mu_0 H$ = 2.2 MT. Though maximum possible MCE in Fe-Rh alloys remains unknown, Ref. [17] reports that increasing the field from 2 to 8 T leads to an increase in MCE of only about 50% (from 13.5 to 20 K).

Table I summarizes the potential magnetocaloric performance of two differently processed samples, where it is clear that the magnetic entropy changes are superior for the fast-quenched sample. The same is true for refrigerant capacities estimated using the following criteria: (i) by finding the product $\left|\Delta S_M^{peak}\right| \times \delta T_{FWHM}$ (referred to as *RC*-1), where $\delta T_{FWHM} = T_{hot} - T_{cold}$, corresponds to the full-width at half-maximum of the $\Delta S_M(T)$ curve; (ii) by calculating the area under the $\Delta S_M(T)$ curve between T_{hot} and T_{cold} (*RC*-2); and (iii) by maximizing the product $\Delta S_M \times \delta T$ below the $\Delta S_M(T)$ curve (*RC*-3; Wood and Potter criterion).

Finally, we have also estimated the magnetic hystereses loss as a function of temperature across the AFM→FM transition for both samples. Figures 7(a) and (b) show the isothermal magnetization curves measured when increasing and decreasing the magnetic field, whereas the thermal dependence of the irreversible loss *HL* for a maximum applied magnetic field of 2 T estimated from the area between the curves, is depicted in Fig. 7(c). It is important to highlight that to measure the isothermal magnetization curves at each temperature we followed the thermal cycle described in the Experimental section; the hysteresis loss at a given *T* was obtained from the area enclosed between the respective field-up and field-down isothermal curves. We note that in spite of both samples showing large values of the maximum hysteresis loss owing to the fast magnetization increase beyond the critical field, the more drastic magnetization change exhibited by the FQ sample leads to substantially larger loss values. The average values of the magnetic hysteresis loss $\langle HL \rangle_{FWHM}$ over δT_{FWHM} for FQ and SC samples were found to be 64 and 37 J kg-1, respectively; even when $\langle HL \rangle_{FWHM}$ is larger for FQ sample it shows a larger effective refrigerant capacity. By comparing hysteresis loss values obtained for FQ and SC $Fe_{49}Rh_{51}$ alloys with slow cooled $Gd_5Ge_2Si_2$ (alloy with giant MCE and hysteretic first-order phase transition) the obtained value of hysteresis loss is about 36 % smaller for SC $Fe_{49}Rh_{51}$ and is about 15 % larger for FQ $Fe_{49}Rh_{51}$ [31]. Additionally, these values are about 19 % smaller and 46 % larger for SC and FQ $Fe_{49}Rh_{51}$ respectively compared with FeRh thin film [32].

4. CONCLUSIONS

Achieving reproducibility and maximizing magnetothermal effects in FeRh alloys requires a better understanding of how varying synthesis parameters affect the magnetostructural transition. This work draws attention to the strong effect that the cooling rate from the thermal annealing temperature has on the magnetocaloric response, refrigerant capacity, and hysteresis loss associated with the first-order AFM↔FM magnetoelastic transition. The cooling rate impacts the phase purity, whereas a rapidly quenched alloy is the nearly phase-pure B2 FeRh, while the face-centered γ-FeRh is the dominant phase in the slowly cooled material. Rapid quenching from the annealing temperature leads to: (a) a sharp AFM↔FM phase transition and large magnetization change from the AFM to the FM state; (b) a high $|\Delta S_M^{peak}|$ and a fast approach of $|\Delta S_M^{peak}|$ to saturation; (c) a table-like $\Delta S_M(T)$ curve (in the present case above 1 T); (d) a large refrigerant capacity, and; (e) a large field-induced average hysteresis loss.

ACKNOWLEDGEMENTS

J.L. Sánchez Llamazares acknowledges the support received from Laboratorio Nacional de Investigaciones en Nanociencias y Nanotecnología (LINAN), IPICYT; the technical support received from M.Sc. B.A. Rivera-Escoto is gratefully acknowledged. Work at Advanced Magnetic Technologies and Consulting, LLC was supported by Skolkovo Foundation, Russia. C.F. Sánchez-Valdés is grateful to DMCU-UACJ for supporting his research stays at IPICyT (program PFCE and academic mobility grant); also, for the financial support received from SEP-Conacyt, Mexico (Grant No. A1-S-37066). Work at Ames Laboratory was supported by the U. S. Department of Energy, Office of Science, Division of Materials Science and Engineering of the Office of Basic Energy Sciences under Contract No. DE-AC02-07CH11358 with Iowa State University.

REFERENCES

[1] S.A. Nikitin, G. Myalikgulyev, A.M. Tishin, M.P. Annaorazov, K.A. Asatryan, A.L. Tyurin, The magnetocaloric effect in Fe49Rh51 compound, Phys. Lett. A. 148 (1990) 363–366. doi:10.1016/0375-9601(90)90819-A.

[2] M.P. Annaorazov, S.A. Nikitin, A.L. Tyurin, K.A. Asatryan, A.K. Dovletov, Anomalously high entropy change in FeRh alloy, J. Appl. Phys. 79 (1996) 1689–1695. doi:10.1063/1.360955.

[3] M.P. Annaorazov, K.A. Asatryan, G. Myalikgulyev, S.A. Nikitin, A.M. Tishin, A.L. Tyurin, Alloys of the Fe-Rh system as a new class of working material for magnetic refrigerators, Cryogenics. 32 (1992) 867–872. doi:10.1016/0011-2275(92)90352-B.

[4] R. Barua, F. Jiménez-Villacorta, L.H. Lewis, Towards tailoring the magnetocaloric response in FeRh-based ternary compounds, J. Appl. Phys. 115 (2014) 17A903. doi:10.1063/1.4854975.

[5] A. Chirkova, K.P. Skokov, L. Schultz, N.V. Baranov, O. Gutfleisch, T.G. Woodcock, Giant adiabatic temperature change in FeRh alloys evidenced by direct measurements under cyclic conditions, Acta Mater. 106 (2016) 15–21. doi:10.1016/j.actamat.2015.11.054.

[6] N.A. Zarkevich, D.D. Johnson, Predicted martensitic and quantified metamagnetic transformations in FeRh, ArXiv170203042 Cond-Mat Physicsphysics. (2017). http://arxiv.org/abs/1702.03042 (accessed March 18, 2017).

[7] J.S. Kouvel, Unusual Nature of the Abrupt Magnetic Transition in FeRh and Its Pseudobinary Variants, J. Appl. Phys. 37 (1966) 1257–1258. doi:10.1063/1.1708424.

[8] A.I. Zakharov, A.M. Kadomtseva, R.Z. Levitin, E.G. Ponyatovskii, Sov. Phys. JETP. 19 (1964) 1348.

[9] L. Muldawer, F. deBergevin, Antiferromagnetic-Ferromagnetic Transformation in FeRh, J. Chem. Phys. 35 (1961) 1904–1905. doi:10.1063/1.1732175.

[10] V.I. Zverev, A.M. Saletsky, R.R. Gimaev, A.M. Tishin, T. Miyanaga, J.B. Staunton, Influence of structural defects on the magnetocaloric effect in the vicinity of the first order magnetic transition in Fe50.4Rh49.6, Appl. Phys. Lett. 108 (2016) 192405. doi:10.1063/1.4949355.

[11] C. Baldasseroni, C. Bordel, A.X. Gray, A.M. Kaiser, F. Kronast, J. Herrero-Albillos, C.M. Schneider, C.S. Fadley, F. Hellman, Temperature-driven nucleation of ferromagnetic domains in FeRh thin films, Appl. Phys. Lett. 100 (2012) 262401. doi:10.1063/1.4730957.

[12] F. Quirin, M. Vattilana, U. Shymanovich, A.-E. El-Kamhawy, A. Tarasevitch, J. Hohlfeld, D. von der Linde, K. Sokolowski-Tinten, Structural dynamics in FeRh during a laser-induced metamagnetic phase transition, Phys. Rev. B. 85 (2012) 020103. doi:10.1103/PhysRevB.85.020103.

[13] S.O. Mariager, F. Pressacco, G. Ingold, A. Caviezel, E. Möhr-Vorobeva, P. Beaud, S.L. Johnson, C.J. Milne, E. Mancini, S. Moyerman, E.E. Fullerton, R. Feidenhans'l, C.H. Back, C. Quitmann, Structural and Magnetic Dynamics of a Laser Induced Phase Transition in FeRh, Phys. Rev. Lett. 108 (2012) 087201. doi:10.1103/PhysRevLett.108.087201.

[14] J.-U. Thiele, S. Maat, J.L. Robertson, E.E. Fullerton, Magnetic and structural properties of FePt-FeRh exchange spring films for thermally assisted magnetic recording media, IEEE Trans. Magn. 40 (2004) 2537–2542. doi:10.1109/TMAG.2004.829325.

[15] D.W. Cooke, F. Hellman, C. Baldasseroni, C. Bordel, S. Moyerman, E.E. Fullerton, Thermodynamic Measurements of Fe-Rh Alloys, Phys. Rev. Lett. 109 (2012) 255901. doi:10.1103/PhysRevLett.109.255901.

[16] W. He, H. Huang, X. Ma, First-principles calculations on elastic and entropy properties in FeRh alloys, Mater. Lett. 195 (2017) 156–158. doi:10.1016/j.matlet.2017.02.043.

[17] A.M. Aliev, A.B. Batdalov, L.N. Khanov, A.P. Kamantsev, V.V. Koledov, A.V. Mashirov, V.G. Shavrov, R.M. Grechishkin, A.R. Kaul', V. Sampath, Reversible magnetocaloric effect in materials with first order phase transitions in cyclic magnetic fields: $Fe_{48}Rh_{52}$ and $Sm_{0.6}Sr_{0.4}MnO_3$, Appl. Phys. Lett. 109 (2016) 202407. doi:10.1063/1.4968241.

[18] J. Liu, T. Gottschall, K.P. Skokov, J.D. Moore, O. Gutfleisch, Giant magnetocaloric effect driven by structural transitions, Nat. Mater. 11 (2012) 620–626. doi:10.1038/nmat3334.
[19] A. Chirkova, F. Bittner, K. Nenkov, N.V. Baranov, L. Schultz, K. Nielsch, T.G. Woodcock, The effect of the microstructure on the antiferromagnetic to ferromagnetic transition in FeRh alloys, Acta Mater. 131 (2017) 31–38. doi:10.1016/j.actamat.2017.04.005.
[20] L.J. Swartzendruber, The Fe−Rh (Iron-Rhodium) system, Bull. Alloy Phase Diagr. 5 (1984) 456–462. doi:10.1007/BF02872896.
[21] J.B. Staunton, R. Banerjee, M. dos S. Dias, A. Deak, L. Szunyogh, Fluctuating local moments, itinerant electrons, and the magnetocaloric effect: Compositional hypersensitivity of FeRh, Phys. Rev. B. 89 (2014) 054427. doi:10.1103/PhysRevB.89.054427.
[22] A.M.G. Carvalho, D.H.C. Araújo, H.F. Canova, C.B. Rodella, D.H. Barrett, S.L. Cuffini, R.N. Costa, R.S. Nunes, X-ray powder diffraction at the XRD1 beamline at LNLS, J. Synchrotron Radiat. 23 (2016) 1501–1506. doi:10.1107/S1600577516012686.
[23] A. Quintana-Nedelcos, J.L. Sánchez Llamazares, C.F. Sánchez-Valdés, P. Álvarez Alonso, P. Gorria, P. Shamba, N.A. Morley, On the correct estimation of the magnetic entropy change across the magneto-structural transition from the Maxwell relation: Study of MnCoGeBx alloy ribbons, J. Alloys Compd. 694 (2017) 1189–1195. doi:10.1016/j.jallcom.2016.10.116.
[24] H. Miyajima, S. Yuasa, Structural phase transition and magnetic properties of FeRh1−xCox alloys, J. Magn. Magn. Mater. 104 (1992) 2025–2026. doi:10.1016/0304-8853(92)91652-A.
[25] J. Balun, L. Eleno, G. Inden, Phase equilibria in the Fe–Rh–Ti system I. Experimental results, Intermetallics. 15 (2007) 1237–1247. doi:10.1016/j.intermet.2007.03.002.
[26] C.C. Chao, P. Duwez, C.C. Tsuei, Metastable fcc Fe–Rh Alloys and the Fe–Rh Phase Diagram, J. Appl. Phys. 42 (1971) 4282–4284. doi:10.1063/1.1659766.
[27] E. Kren, L. Pal, P. Szabo, Neutron diffraction investigation of the antiferromagnetic-ferromagnetic transformation in the FeRh alloy, Phys. Lett. 9 (1964) 297–298. doi:10.1016/0031-9163(64)90369-5.
[28] M.R. Ibarra, P.A. Algarabel, Giant volume magnetostriction in the FeRh alloy, Phys. Rev. B. 50 (1994) 4196–4199. doi:10.1103/PhysRevB.50.4196.
[29] J.B. McKinnon, D. Melville, E.W. Lee, The antiferromagnetic-ferromagnetic transition in iron-rhodium alloys, J. Phys. C Solid State Phys. 3 (1970) S46. doi:10.1088/0022-3719/3/1S/306.
[30] A.M. Tishin, Magnetocaloric effect in strong magnetic fields, Cryogenics. 30 (1990) 127–136. doi:10.1016/0011-2275(90)90258-E.
[31] V. Provenzano, A.J. Shapiro, R.D. Shull, Reduction of hysteresis losses in the magnetic refrigerant Gd5Ge2Si2 by the addition of iron, Nature. 429 (2004) 853–857. doi:10.1038/nature02657.
[32] Y. Liu, L.C. Phillips, R. Mattana, M. Bibes, A. Barthélémy, B. Dkhil, Large reversible caloric effect in FeRh thin films via a dual-stimulus multicaloric cycle, Nat. Commun. 7 (2016). doi:10.1038/ncomms11614.
[33] M. Manekar, S.B. Roy, Reproducible room temperature giant magnetocaloric effect in Fe?Rh, J. Phys. Appl. Phys. 41 (2008) 192004. doi:10.1088/0022-3727/41/19/192004.

FIGURE CAPTIONS

Fig. 1. Room temperature X-ray powder diffraction patterns [(a) and (b)] and thermal dependence of unit cell lattice parameter *a* [(c)] for FQ and SC $Fe_{49}Rh_{51}$ samples.

Fig. 2. ZFCW and FC $M(T)$ curves measured under a static applied magnetic field of 5 mT and heating/cooling DSC curves for FQ (a) and SC (b) $Fe_{49}Rh_{51}$ samples. AF_S (FA_S) refers to the starting temperature of the AFM → FM (FM → AFM) transition.

Fig. 3. Temperature dependencies of magnetization measured in 5 mT magnetic field during warming after zero-field cooling (ZFCW) and during field cooling (FC) for FQ (a) and SC $Fe_{49}Rh_{51}$ (b). Top insets: low magnetization details around and below the magnetoelastic transition. Bottom insets: dM/dT in the vicinity of T_C.

Fig. 4. ZFCW and FC $M(T)$ curves measured under a static applied magnetic field of 2 T for $Fe_{49}Rh_{51}$ samples annealed at 1273 K during 48 hours after fast quenching (FQ) into iced-water (black circles) a slow cooling (SC) at 2 K/min to RT (red triangles). Inset: temperature dependence of dM/dT.

Fig. 5. (a) Comparison of the isothermal magnetization curves $M(\mu_o H)$ measured across the AFM-to-FM transition for the fast quenched (310-345 K) and slow cooled (310-360 K) $Fe_{49}Rh_{51}$ samples up to a maximum applied magnetic field of 2 T. (b) Temperature dependence of the critical fields $\mu_o H_{cr}$ obtained from $M(\mu_o H)$ curves for FQ (blue open squares) and SC (red filled circles) $Fe_{49}Rh_{51}$ samples.

Fig. 6. (a) Temperature dependence of the magnetic entropy change ΔS_M at selected magnetic field values up to 2 T for the fast quenched (FQ) and slow cooled (SC) $Fe_{49}Rh_{51}$ samples. (b) Maximum value of the magnetic entropy change $|\Delta S_M^{peak}|$ as a function of the magnetic field change for the fast quenched (FQ) and slow cooled (SC) $Fe_{49}Rh_{51}$ samples. Inset: magnetic field change dependence of $\Delta S_M^{peak}/\Delta S_M^{max}$. (c) Magnetic field change dependence of the T_{cold}, T_{hot} and δT_{FWHM} for both alloys.

Fig. 7. Isothermal magnetization curves $M(\mu_o H)$ measured at selected temperatures across the AFM-to-FM transition on increasing and decreasing the magnetic field up to 2 T for FQ (a) and SC (b) $Fe_{49}Rh_{51}$ bulk alloys. (c) Temperature dependence of the magnetic hysteresis loss at 2 T for both alloys.

TABLE CAPTIONS

Table I. Maximum value of the magnetic entropy change ΔS_M^{peak}, refrigerant capacity *RC* (see text for definition of *RC*-1, *RC*-2 and *RC*-3), average hysteresis loss $\langle HL \rangle_{FWHM}$ over the full-width at half-maximum of the $\Delta S_M(T)$ curve for the studied FQ and SC $Fe_{49}Rh_{51}$ bulk alloys.

Table I.

$\mu_o \Delta H$ (T)	0.5		1.0		1.5		2.0	
Sample	FQ	SC	FQ	SC	FQ	SC	FQ	SC
$\lvert \Delta S_M^{peak} \rvert$ (J kg^{-1} K^{-1})	10.5	3.0	12.1	5.7	13.2	7.7	13.9*	8.9*
RC-1 (J kg^{-1})	43	24	102	63	167	109	233	162
RC-2 (J kg^{-1})	36	18	91	51	152	90	214	135
$\langle HL \rangle_{FWHM}$ (J kg^{-1})	-	-	-	-	-	-	- 64	- 37
δT_{FWHM} (K)	4	8	8	11	13	14	17	18
T_{hot} (K)	327	330	327	330	327	330	327	330
T_{cold} (K)	323	322	319	319	314	316	310	312
RC-3 (J kg^{-1})	23	16	65	33	114	56	169	86
δT_{FWHM}^{RC-3} (K)	4	31	6	27	10	12	15	15

* In literature, $\lvert \Delta S_M^{peak} \rvert$ has been reported to be 20 J kg^{-1} K^{-1} [3] or 13.6 J kg^{-1} K^{-1} [5] at 2 T for FQ bulk alloys meanwhile 6.5 J kg^{-1} K^{-1} at 2 T [1] or 10 J kg^{-1} K^{-1} at 5 T [33] for SC bulk alloys.

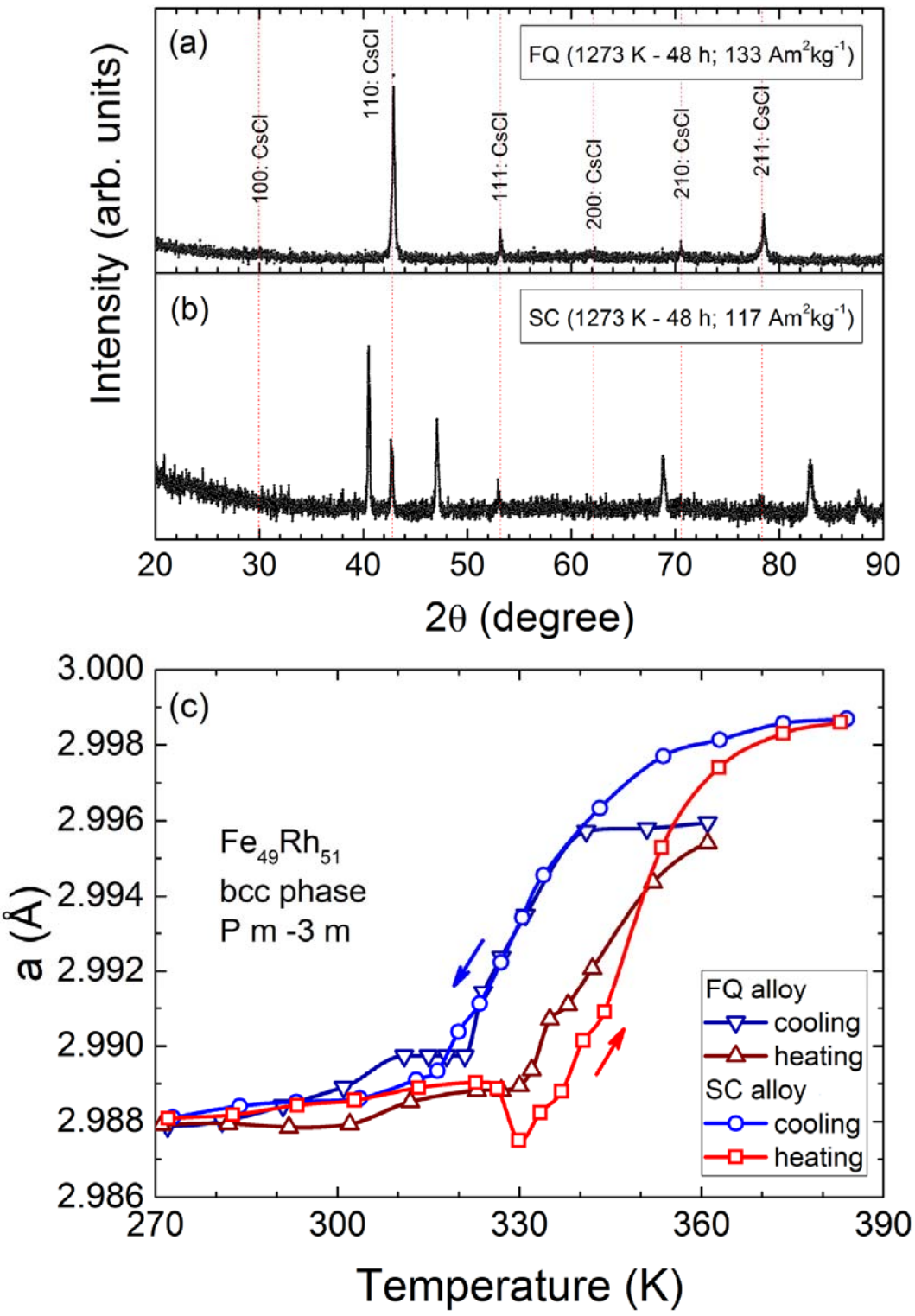
(a)
FQ (1273 K - 48 h; 133 Am²kg⁻¹)
100: CsCl
110: CsCl
111: CsCl
200: CsCl
210: CsCl
211: CsCl
(b)
SC (1273 K - 48 h; 117 Am²kg⁻¹)
Intensity (arb. units)
20
30
40
50
60
70
80
90
2θ (degree)
(c)
Fe49Rh51
bcc phase
P m -3 m
FQ alloy
cooling
heating
SC alloy
cooling
heating
a (Å)
3.000
2.998
2.996
2.994
2.992
2.990
2.988
2.986
270
300
330
360
390
Temperature (K)

Fig. 1.

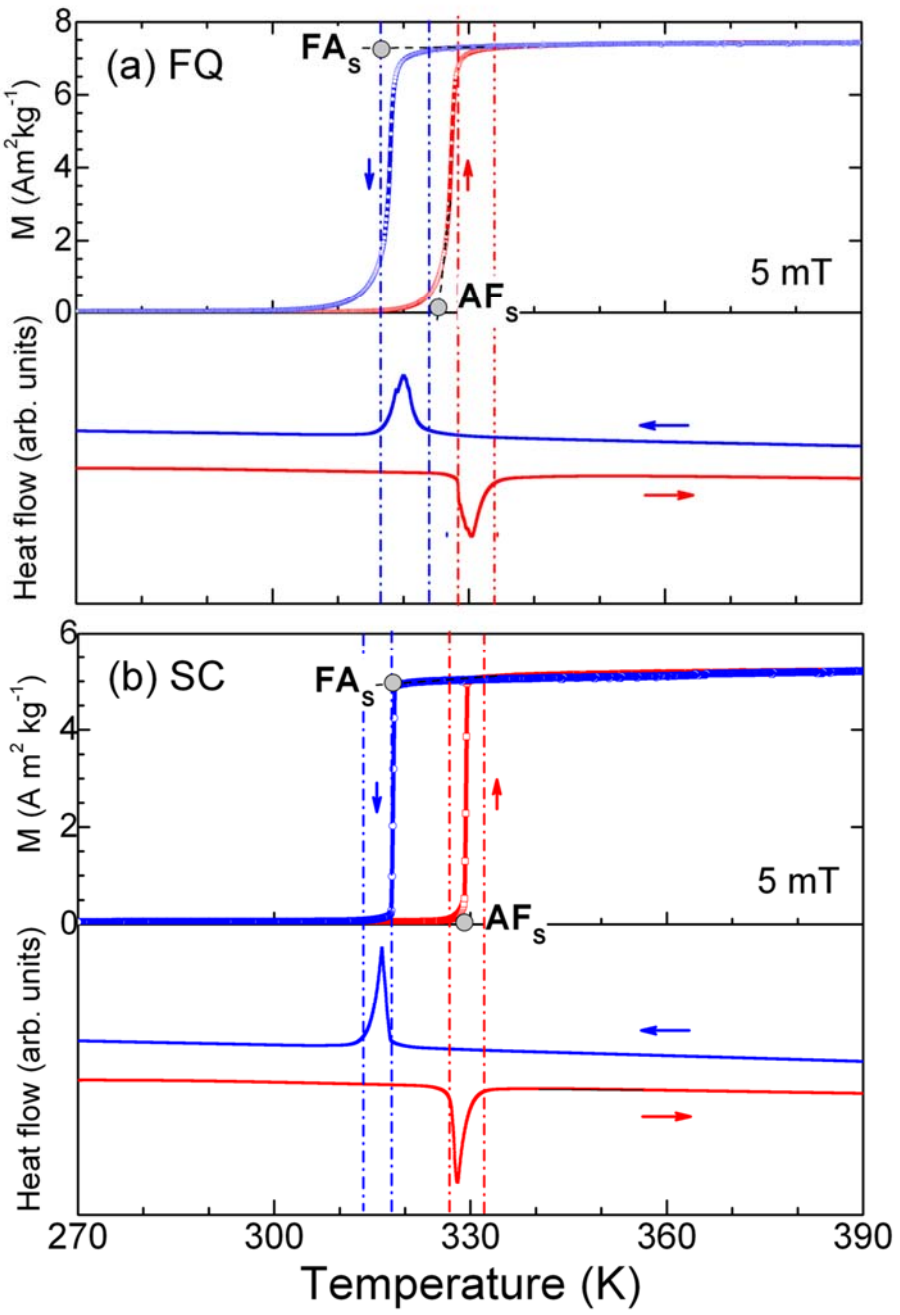
(a) FQ
FA$_s$
AF$_s$
5 mT
M (Am^{2}kg^{-1})
Heat flow (arb. units)
(b) SC
FA$_s$
AF$_s$
5 mT
M (A m^2 kg^{-1})
Heat flow (arb. units)
270
300
330
360
390
Temperature (K)

Fig. 2.

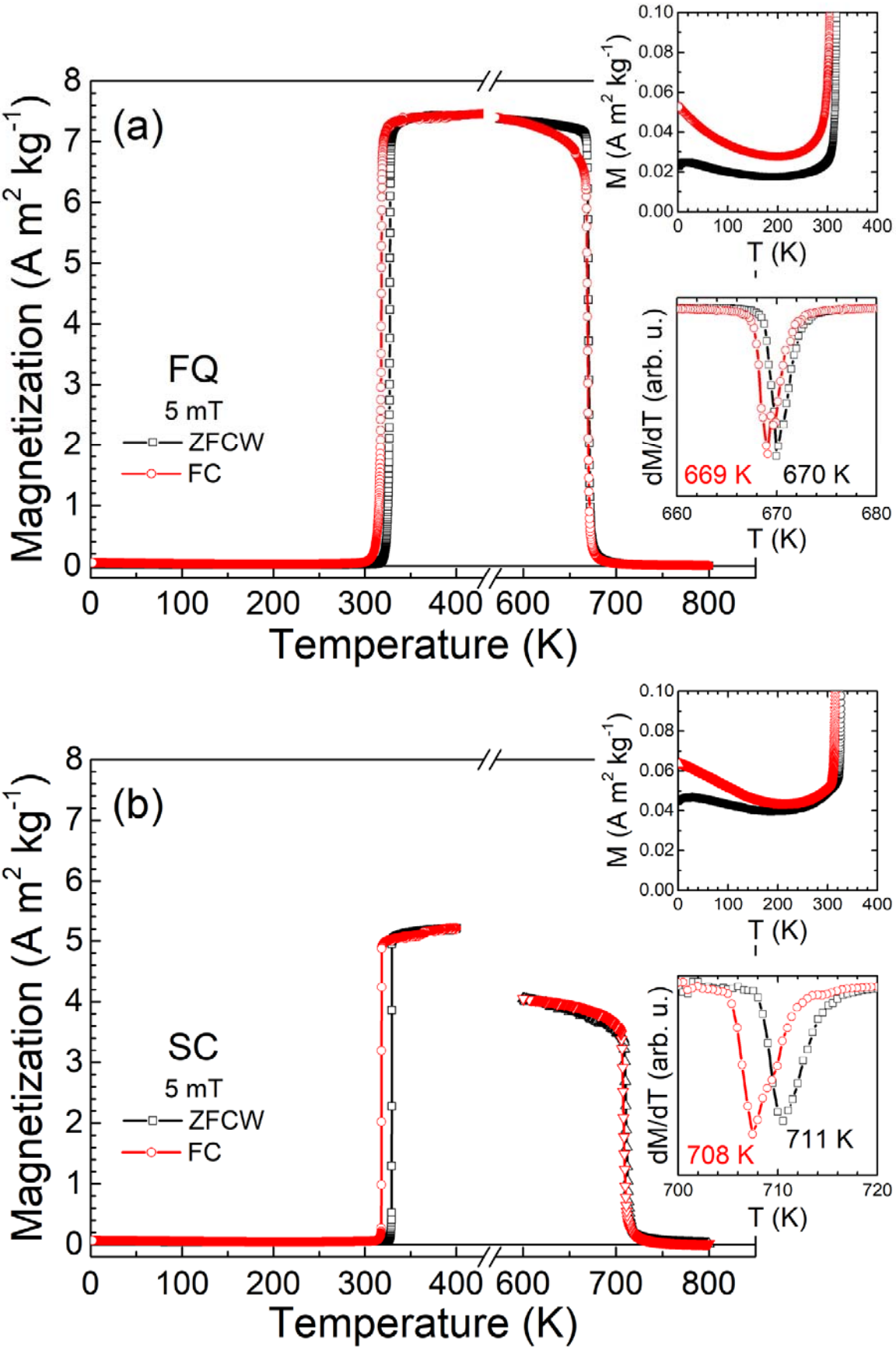
(a)
FQ
5 mT
ZFCW
FC
Magnetization (A m^2 kg^{-1})
Temperature (K)
M (A m^2 kg^{-1})
T (K)
dM/dT (arb. u.)
669 K
670 K
(b)
SC
5 mT
ZFCW
FC
Magnetization (A m^2 kg^{-1})
Temperature (K)
M (A m^2 kg^{-1})
T (K)
dM/dT (arb. u.)
708 K
711 K

Fig. 3.

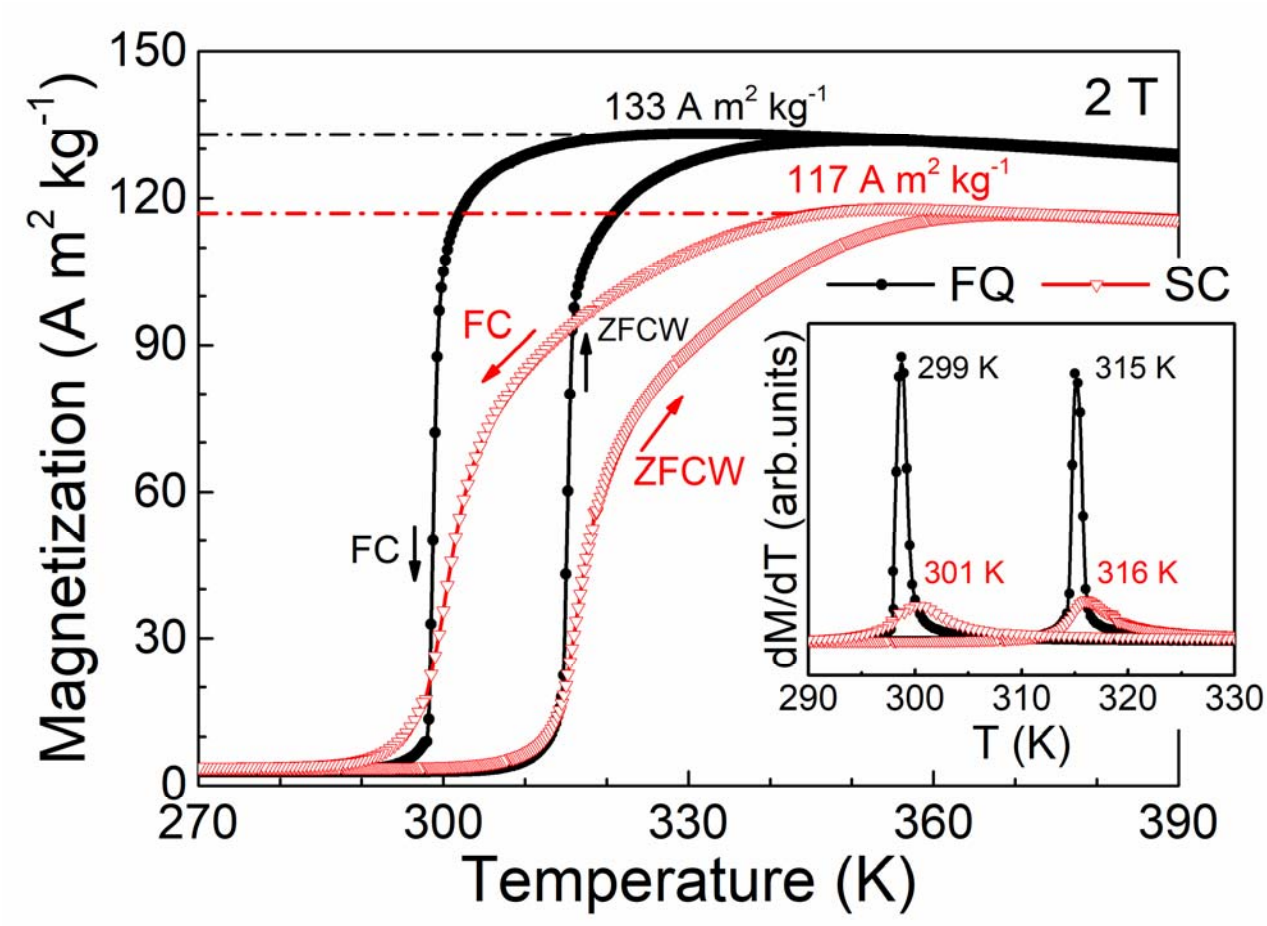
Magnetization (A m^2 kg^{-1})
Temperature (K)
133 A m^2 kg^{-1}
117 A m^2 kg^{-1}
2 T
FQ
SC
FC
ZFCW
FC
ZFCW
dM/dT (arb.units)
299 K
315 K
301 K
316 K
T (K)

Fig. 4.

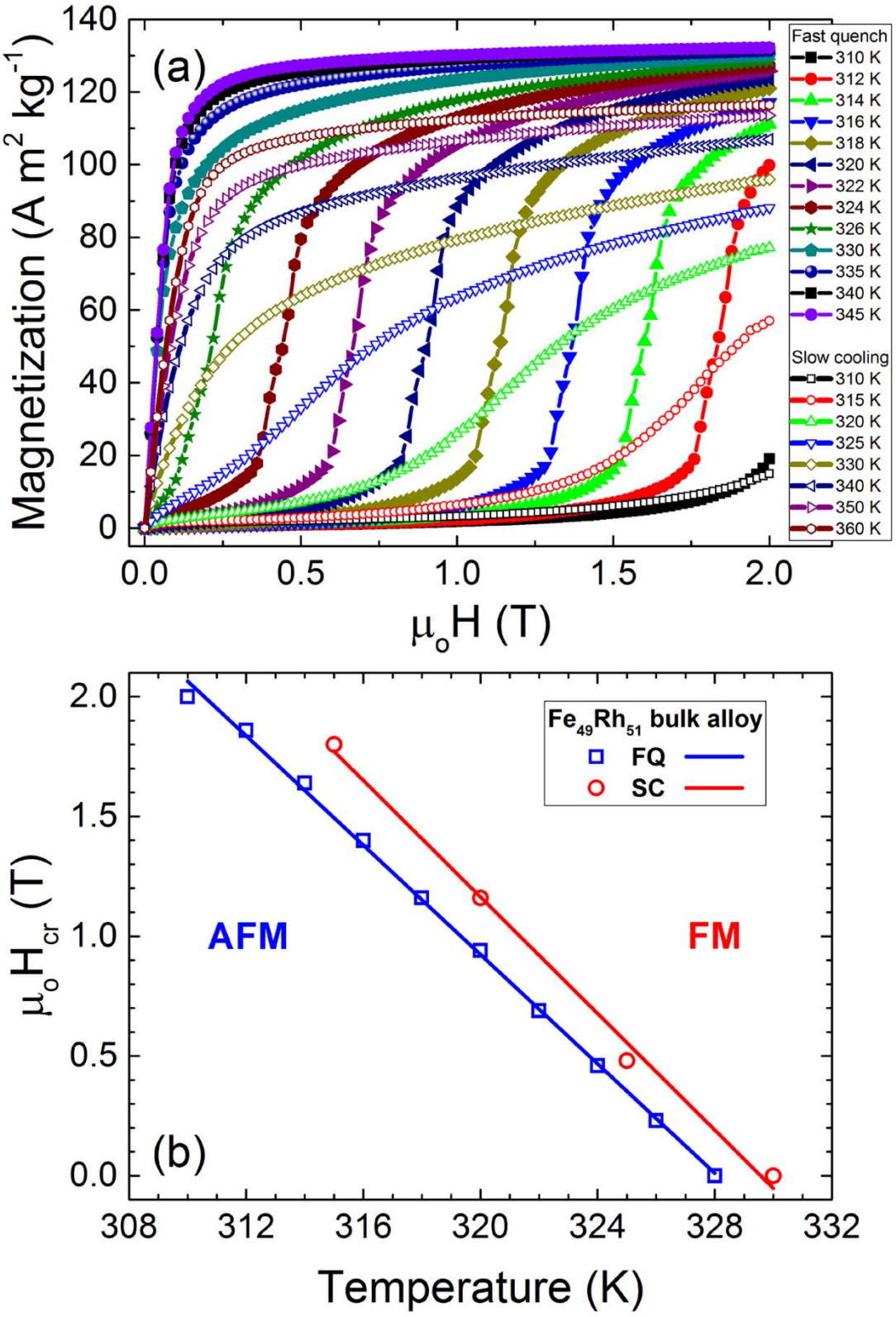
(a)
Magnetization (A m^2 kg^{-1})
μ_oH (T)
Fast quench
310 K
312 K
314 K
316 K
318 K
320 K
322 K
324 K
326 K
330 K
335 K
340 K
345 K
Slow cooling
310 K
315 K
320 K
325 K
330 K
340 K
350 K
360 K
(b)
$\mu_o H_{cr}$ (T)
Temperature (K)
$Fe_{49}Rh_{51}$ bulk alloy
FQ
SC
AFM
FM

Fig. 5.

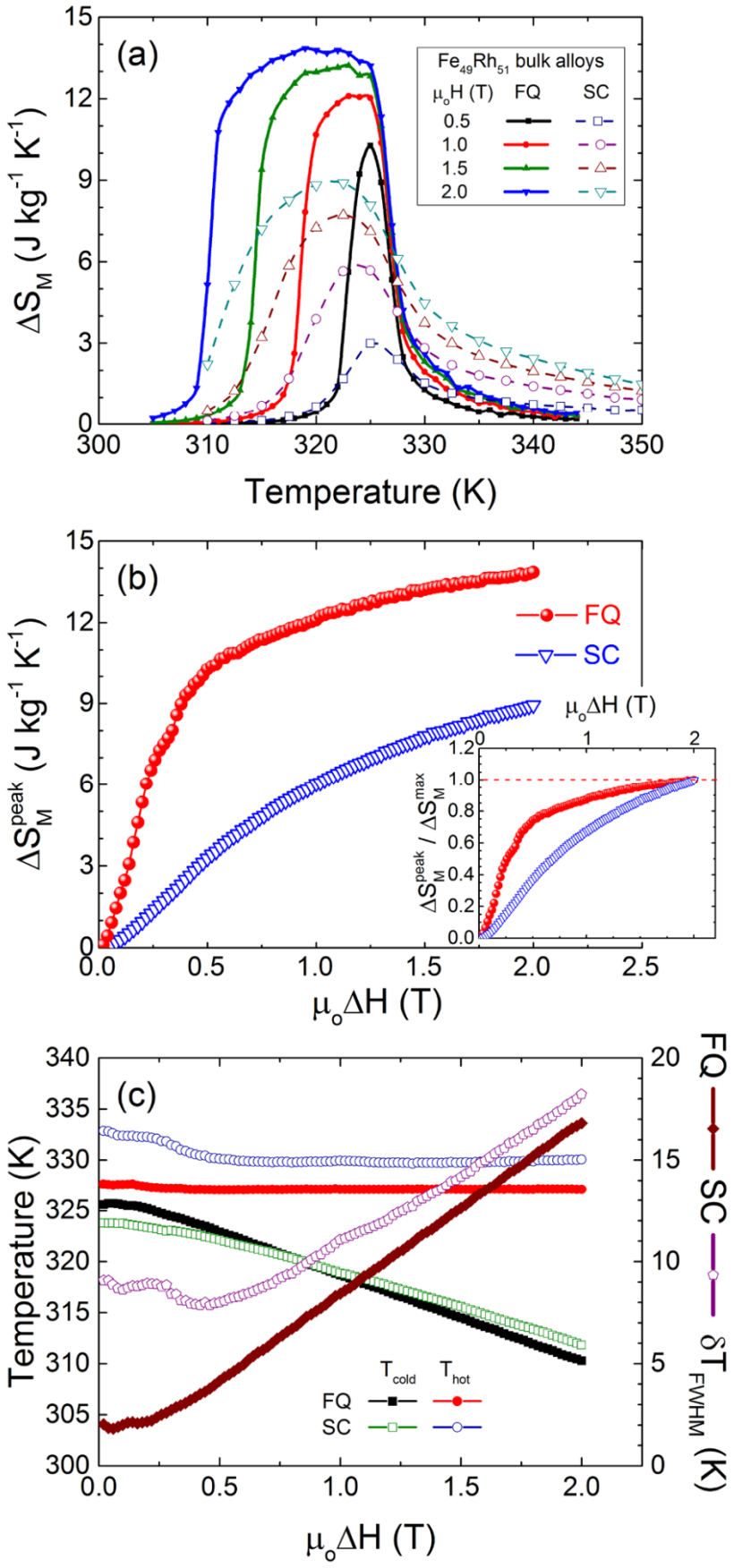
(a)
Fe49Rh51 bulk alloys
μoH (T) FQ SC
0.5
1.0
1.5
2.0
ΔSM (J kg-1 K-1)
Temperature (K)
(b)
FQ
SC
μoΔH (T)
ΔSMpeak (J kg-1 K-1)
ΔSMpeak / ΔSMmax
μoΔH (T)
(c)
Temperature (K)
Tcold Thot
FQ
SC
FQ
SC
δTFWHM (K)
μoΔH (T)

Fig. 6.

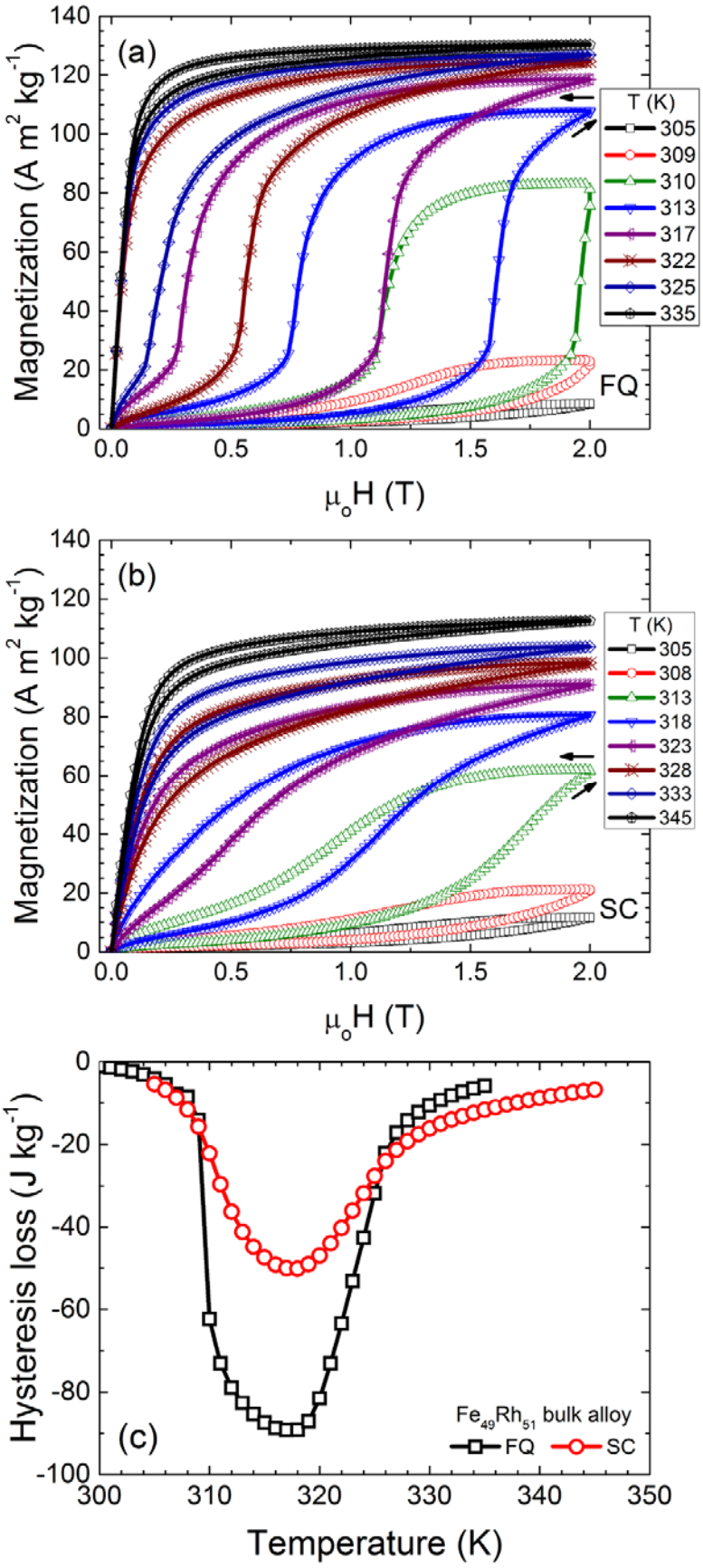
(a)
Magnetization (A m^2 kg^{-1})
μ_oH (T)
T (K)
305
309
310
313
317
322
325
335
FQ
(b)
Magnetization (A m^2 kg^{-1})
μ_oH (T)
T (K)
305
308
313
318
323
328
333
345
SC
(c)
Hysteresis loss (J kg^{-1})
Temperature (K)
$Fe_{49}Rh_{51}$ bulk alloy
FQ
SC

Fig. 7.